Tutor/s

Dra. Anna de Juan Capdevila
Departament de Química Analítica

Dra. Maria Marsal Terés
Institut de Ciències Fotòniques (ICFO)

Grau de Química

Treball Final de Grau

Combined use of hyperspectral imaging and chemometrics to investigate the development of zebrafish embryos.

Ús combinat de la imatgeria hiperespectral i la quimiometria per a l'estudi del desenvolupament embrionari del peix zebra.

Berta Pons Forrellat

January 2026

Universitat de Barcelona

B:KC Barcelona Knowledge Campus
Campus d'Excel·lència Internacional

The important thing is not to stop questioning. Curiosity has its own reason for existing.

Albert Einstein

A l'Anna i la Maria, gràcies per ser dues tutores excepcionals, per ajudar-me tant durant tots aquests mesos, transmetent-me tot el vostre coneixement, resolent tots els meus dubtes i permetent-me aprendre tant de vosaltres.

A la resta de companys de l'ICFO, gràcies per acollir-me tant bé al vostre grup i per ajudar-me amb qualsevol cosa, sempre amb un somriure.

A l'Albert, gràcies per ajudar-me des del primer dia amb tots els dubtes que he tingut del MATLAB (que no han sigut pocs) i per totes les hores compartides tant al ICFO com al laboratori de la uni.

A les meves companyes de la uni, Laura, Elna i Ruth, gràcies per acompanyar-me durant aquests 4 anys, que no han estat fàcils, però amb vosaltres han sigut molt especials.

A la meva família, gràcies pel vostre suport incondicional, per creure sempre amb mi i donar-me força en els moments més complicats.

Aquest treball és per a tots vosaltres.

REPORT

IDENTIFICATION AND REFLECTION ON THE SUSTAINABLE DEVELOPMENT GOALS (SDG)

This project explores the application of hyperspectral imaging combined with chemometric methods to study zebrafish embryonic development. Understanding development in this species is particularly important, since zebrafish shares a high degree of genetic similarity with humans, providing valuable insights into human diseases and potential strategies for their treatment.[1]

The Sustainable Development Goals (SDGs) addressed in this project belong to the People and Partnership categories, since they focus on health, scientific research and collaborative efforts. This thesis aligns with the following SDGs, which reflect best its objectives:

- SDG 3: good health and well-being
  This goal promotes better health through prevention, early diagnosis and improved medical tools. My thesis contributes to this goal by using zebrafish embryos, hyperspectral imaging and chemometrics to detect biological changes in a non-invasive way. Since zebrafish is a key biomedical model, this approach helps advance methods that ultimately protect human health.

- SDG 17: partnerships
  This goal highlights that collaboration between institutions is essential to address global challenges. In this case, the partnership between the University of Barcelona (UB) and the Institut de Ciències Fotòniques (ICFO) in my thesis reflects this goal directly: both institutions share knowledge and resources to improve the quality and impact of the project. This cooperation exemplifies how effective alliances contribute to scientific progress and support the achievement of SDGs.

ICFO activities clearly align with the 2030 Agenda, particularly SDGs 3 and 17. Through the “Light for Health” initiative, this institution promotes applied research, innovation, and interdisciplinary collaboration, demonstrating how scientific institutions can contribute directly to sustainable and global health goals.[2]

This project has the potential to be developed into a larger-scale study in the future, since there is still much to explore in these embryos and further investigations could provide new insights into the dynamics of lipid distribution, cellular processes and morphogenetic movements. Such findings may not only enhance our fundamental knowledge of developmental biology but could also have a broader impact on human health.

CONTENTS

1. SUMMARY

Zebrafish (*Danio rerio*) is a widely used model organism in biological research due to its high genetic similarity to humans. The optical transparency of the embryos, easy accessibility and fast development are the characteristics that make zebrafish particularly suitable for developmental and biomedical research.

This project will focus on the investigation of the lipid distribution during zebrafish embryonic development, specifically at the middle-epiboly stage. To achieve this goal, embryos were stained using two lipidic-selective fluorophores, Nile Red and Lipi-Green, and analysed using confocal fluorescence hyperspectral imaging. Initially, embryos were stained with a single fluorophore at a time to evaluate its specificity and distribution. Subsequently, both fluorophores were applied simultaneously to enable a combined analysis of lipid components across the different embryonic regions. Due to the large and complex nature of hyperspectral datasets, chemometric analysis based on Multivariate Curve Resolution – Alternating Least Squares (MCR-ALS) was applied to extract meaningful information, obtaining the pure spectral signatures and the spatial distribution of the different lipid components.

The results showed that Nile Red stained the three main embryonic regions – the yolk, the yolk syncytial layer (YSL) and the embryonic cells –, exhibiting two distinct emission shifts associated with differences in lipid polarity of the components. In contrast, Lipi-Green labelled a single lipid component, present in specific parts of the three regions.

Overall, this study demonstrates that the combination of fluorescence hyperspectral imaging and chemometric analysis is a powerful approach for characterizing chemical and morphological changes during zebrafish embryonic development.

Keywords: Zebrafish, embryonic development, lipidic-selective fluorophores, confocal fluorescence hyperspectral imaging, chemometrics, MCR-ALS.

2. RESUM

El peix zebra (*Danio rerio*) és un organisme model àmpliament utilitzat en la recerca biològica a causa de la seva elevada similitud genètica amb els humans. La seva transparència òptica dels embrions, la seva fàcil accessibilitat i el seu desenvolupament ràpid són característiques que fan que del peix zebra un model especialment adequat per a estudis del desenvolupament embrionari i la recerca biomèdica.

Aquest projecte se centra en l'estudi de la distribució lipídica durant el desenvolupament embrionari del peix zebra, específicament en l'etapa d'epibòlia del 50%. Per aconseguir aquest objectiu, els embrions van ser tenyits amb dos fluoròfors selectius de lípids, Nile Red i Lipi-Green, i analitzats mitjançant imatges hiperespectrals de fluorescència confocal. Inicialment, els embrions es van tenyir amb cada un dels dos fluoròfors per separat per avaluar-ne l'especificitat i la distribució. Posteriorment, es van aplicar ambdós fluoròfors simultàniament per permetre una anàlisi combinada dels components lipídics a les diferents regions embrionàries. A causa de la grandària i la natura dels conjunts de dades hiperespectrals, es va aplicar una anàlisi quimiomètrica basada en el mètode de Resolució Multivariant de Corbes per Mínims Quadrats Alternats (MCR-ALS) per extreure informació rellevant de les mostres analitzades i obtenir les signatures espectrals pures i la distribució espacial dels diferents components lipídics.

Els resultats van mostrar que el Nile Red tenyia les tres principals regions embrionàries – el sac vitel·lí, la capa sincicial del sac vitel·lí (YSL) i les cèl·lules embrionàries –, mostrant dues signatures espectrals d'emissió diferenciades associades a components lipídics de diferent polaritat. En canvi, el Lipi-Green marcava un únic component lipídic, present en parts específiques de les tres regions.

En conjunt, aquest estudi demostra que la combinació d'imatges hiperespectrals de fluorescència i ànalisi quimiomètrica constitueix una aproximació molt potent per caracteritzar els canvis químics i morfològics durant el desenvolupament embrionari del peix zebra.

Paraules clau: Peix zebra, desenvolupament embrionari, fluoròfors selectius de lípids, imatges hiperespectrals de fluorescència confocal, quimiometria, MCR-ALS.

3. INTRODUCTION

Zebrafish (*Danio rerio*) is a small tropical freshwater fish, whose name comes from the horizontal stripes on their bodies. Even though they are very different from humans, approximately 70% of human genes are also present in zebrafish.[3] They share a lot of features with humans such as two eyes, brain, spinal cord, intestine, pancreas, liver, heart, kidney… The use of zebrafish to study genetic causes of human diseases is increasing due to their fast development, easy accessibility and optically clear embryos, establishing them as a powerful and widely used model organism. For this reason, understanding zebrafish embryonic development is highly relevant.

After fertilization, the zebrafish embryo consists of a single cell located on top of a large yolk cell. Cell divisions occur only on the animal pole, while the yolk does not divide. During early development, embryonic cells undergo synchronous and symmetric cleavage divisions, leading to a progressive doubling in cell number (see Figure 1). These divisions form the blastoderm, a group of cells located above the yolk known as blastomeres, which are the progenitor cells that will give rise to the body.[4]

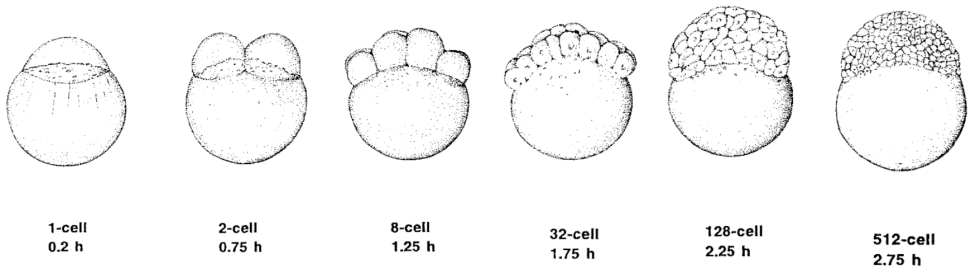

Figure 1. Zebrafish embryo division stages as a function of time after fertilization. (extracted from ref. 4)

Between the ninth and tenth division, some marginal cells collapse and release their nuclei and cytoplasm into the yolk, leading to the formation of the yolk syncytial layer (YSL).[5] This layer plays a crucial role in zebrafish development, as it undergoes highly dynamic movements that are coordinated with the blastoderm.

Epiboly is a morphogenetic movement in the embryo development which involves tissue thinning and spreading of the blastoderm, as shown in Figure 2. It is a key process where the enveloping layer (EVL), the cell layer and the YSL expand to cover the yolk and close the blastopore. This process begins with the yolk cell doming, where deep cells are reorganized, contributing to early embryonic morphogenesis, and ends when the EVL entirely surrounds the yolk. [6]

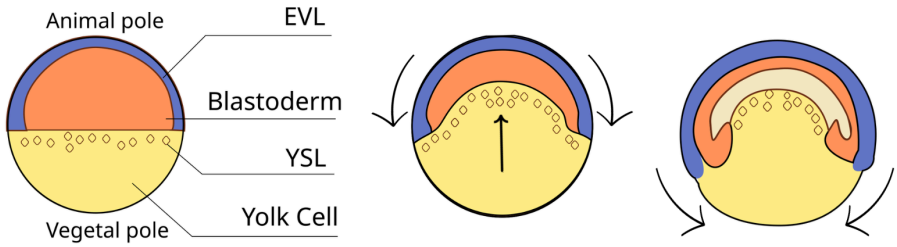

Figure 2. Zebrafish embryo parts and process of epiboly. (extracted from ref. 7)

For this study, we focused on the 50% epiboly stage, which occurs when the YSL reaches the equator of the yolk. This process takes places around 5.3 hours post-fertilization.[4] This stage was chosen because the three distinct parts of the embryo (YSL, cells and yolk) are clearly distinguishable, allowing us to study the lipid composition of each part individually. To understand the embryo growth, it is highly relevant to understand the lipid composition differences among the yolk, the animal cell envelope and, particularly, the YSL.

To study the lipid composition in biological tissues, fluorescence labelling is a very suitable option.[8] The smart selection of fluorophores is crucial, since they selectively label different type of lipids according to their chemical nature and provide an effective way to distinguish them. It is known that Nile Red and Lipi-Green are fluorophores that selectively label lipids and have been

successfully used in previous zebrafish studies.[9,10] These fluorophores were selected because they stain different lipid species in cells and zebrafish larvae, according to the literature. Nile Red is able to stain both more and less polar lipids, since its emission spectrum varies with the polarity of the environment, allowing different lipid types to be distinguished using a single fluorophore.[11] In contrast, Lipi-Green is expected to preferentially stain lipid droplets, which are mainly composed of neutral lipids.[12] Nevertheless, its behaviour during epiboly stage is not known and therefore requires further investigation.

To localize the different types of stained structures in the embryo, images with spatial and chemical information are required. A suitable technique for this purpose is fluorescence hyperspectral imaging (HSI), which records a fluorescent signal per every pixel of the sample area scanned and, hence, allows a detailed visualization and analysis of lipid location.

Since the acquired HSI images are large and complex, a powerful chemometric method is required to extract useful information. Among the large variety of chemometric tools, unmixing methods such as Multivariate Curve Resolution-Alternating Least Squares (MCR-ALS) are the most suitable option, since they allow identifying the distinct fluorophore spectral signatures of the different dyes applied to the sample and relating this information to the spatial distribution of each component across the image.[13]

4. OBJECTIVES

The principal objective of this study is to understand the lipidic distribution during zebrafish embryonic development, specifically during middle-epiboly stage. To achieve this general objective, the following steps will be undertaken:

- Test the potential of different fluorophores that selectively label lipids, such as Nile Red and Lipi-Green, and establish the analytical conditions related to the staining process.

- Use a confocal fluorescence microscope to acquire hyperspectral images (HSI). In this step, different modalities of fluorescence imaging will be used and instrumental parameters and sample preparation will be optimized.

- Apply an image unmixing method to extract meaningful information from the images to identify the spectral signatures and the spatial distribution of the different lipids in the samples. This step will be crucial to infer the final conclusions and knowledge about the nature and location of the lipids in the different biological structures of zebrafish embryos.

5. EXPERIMENTAL SECTION

5.1. SAMPLE PREPARATION

Zebrafish embryos (wild type) were fertilized at the *Parc de Recerca Biomèdica de Barcelona* and transported into the ICFO installations. Once there, all the experimental procedure for sample preparation started, as displayed in Figure 3. Embryos were incubated at 29ºC until the desired stage, determined by observing them under a microscope to estimate the required time to reach the 50% epiboly stage. Then, they were fixed with a 4% paraformaldehyde (PFA) in phosphate-buffered saline (PBS) solution overnight at 4ºC.

The next step was to remove the PFA by adding PBS and shaking at the orbital shaker for 15 minutes. This was repeated 3 times to make sure there was no PFA left in the solution. After that, the fixed embryos were dechorionated, i.e., the outer layer of the embryo was removed, using fine-tip tweezers to facilitate the fluorescent labelling and imaging.

Subsequently, in some cases, a permeabilization and blocking solution was prepared, consisting of 1% Bovine Serum Albumin (BSA) and 0.3% Triton X-100 in PBS. This solution is used to facilitate the penetration of the labelling agents inside the embryo and to prevent their linking to unspecific sites. The solution was added and stirred for 1 hour, followed by 3 PBS washes as described before.[14]

The last step was to dye the fixed embryos with the desired fluorophore solution for the specified time. In this study, the embryos were labelled using Nile Red and Lipi-Green, which are used as lipid markers. For Nile Red, the embryos were stained with 25 µL of the stock solution (113 µM) of the dye (Thermo Fischer) in 1 mL of PBS for 1 hour. For Lipi-Green, 25 µL of the stock solution (0.1mM) of the dye (DOJINDO) were used for 15 minutes.[10] In the samples where both fluorophores are present, staining was first performed with Lipi-Green and then with Nile Red, following the same procedure as before. Afterwards, they were washed again for 3 times and stored at 4ºC protected from light using aluminium foil, to prevent photobleaching, until the image acquisition.

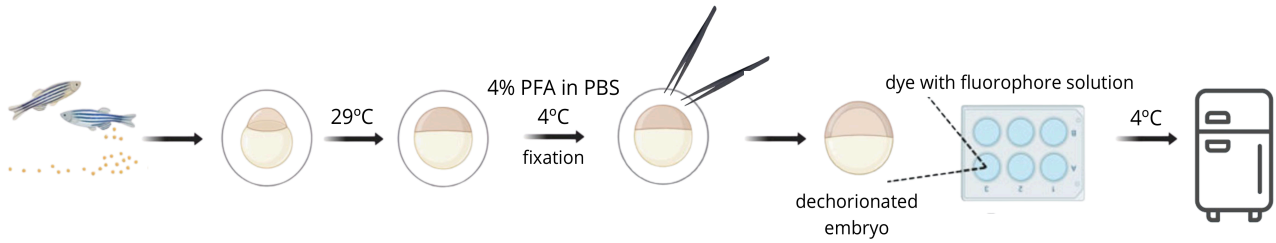

Figure 3. Schematic representation of zebrafish embryo sample preparation.

5.2. IMAGE ACQUISITION

For observation under the microscope, the fixed and labelled embryos were introduced on glass-bottom dishes (Mattek) in a 1% low-melting agarose solution in PBS. Each embryo was oriented using a fine brush to ensure that the YSL was visible and correctly positioned for microscopy. When the agarose solution was solidified, a small amount of PBS was added on top to prevent crackings on the sample.

To analyse the samples, fluorescence confocal microscopy was used. The measurement obtained is a fluorescence image obtained on a sample surface, where every pixel is associated with a fluorescence signal. This technique employs a laser as the light source to control the depth of field, and a pinhole to eliminate out-of-focus light, allowing the visualization of a clear image in a single horizontal plane. This technique allows scanning a single surface plane or several of them, providing a three-dimensional study of samples, including the examination of their internal structure. The samples used in this work must be stained with fluorescent dyes, which are excited by a laser beam and emit light, which is then detected.

Fluorescence images were acquired using a super-resolution and confocal fluorescence microscope, a LEICA TCS SP8 STED 3X microscope.[15] Excitation light was provided by a white laser, the intensity and frame accumulations of which were adjusted to improve image visualization. For Nile Red, the laser was set to an excitation wavelength of 532 nm to match the maximum peak excitation of the dye, whereas for Lipi-Green, it was set to 498 nm.[16,17] For samples with both fluorophores, the laser was set to 498 nm. The

excitation and emission spectra of both dyes can be found in Appendix 1. The light was focused through a 10x objective, and emission was detected using a Gated HyD hybrid detector in the photon-counting mode.

Two types of images were acquired using the xyz and xyλ acquisition modes. The **xyz acquisition** mode enables the capture of images at multiple sample planes, which can then be combined to generate a three-dimensional reconstruction. The signal recorded at each pixel is a single value, representing the integrated fluorescence over the selected emission range. These images were collected to perform an initial analytical assessment of the labelling capacity of each dye and the location of the labelled sample structures. The detection range was set from 10 nm above the excitation wavelength of each fluorophore up to 750 nm.

In contrast, the **xyλ acquisition** mode was used to capture images in a single two-dimensional plane, but the detector measures fluorescence across several wavelength channels. In this case, each pixel is associated with a full emission spectrum, and the image is stored as a data cube, which will be processed using hyperspectral image analysis. The emission spectra were recorded from 10 nm above the excitation wavelength up to 745 nm, in 5 nm increments. Images were captured with a pixel size of 200 x 200 nm. The total scanned area is approximately 0,068mm^2. The image plane scanned was set at the surface of the embryo, and selected so that a region including the yolk, the YSL and the animal cell compartment was recorded in the image.

6. DATA TREATMENT

The result of measuring a hyperspectral image (HSI) in the xyλ mode is a 3-D dataset, known as image hypercube, with the structure xyλ.[18] x and y represent the spatial information, i.e., the pixel coordinates, and λ represents the wavelengths of the spectral dimension, as seen in Figure 4. Data treatment is necessary to extract meaningful information, which includes steps such as preprocessing and multivariate analysis to interpret the complex dataset accurately.

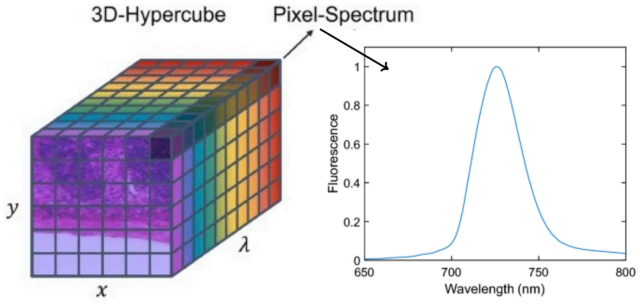

Figure 4. Spectral hypercube representation with the two spatial directions and the spectral dimension. An emission spectrum is obtained per each pixel. (extracted from ref. 19)

6.1. PREPROCESSING

Since the data obtained are large and very complex, image preprocessing is required. Spatial binning is done by averaging the neighbouring pixels in a certain window area, e.g., 2 x 2 pixels, to obtain a single spectrum associated with the total binned area. Spatial binning is performed in order to decrease image size and increase the signal-to-noise ratio of spectra. For all the images in this work, an 8 x 8 binning was applied to reduce the dimensionality of the data collected, without losing a lot of spatial resolution, as shown in Figure 5. The final binned pixel size obtained was 1600 x 1600 nm.

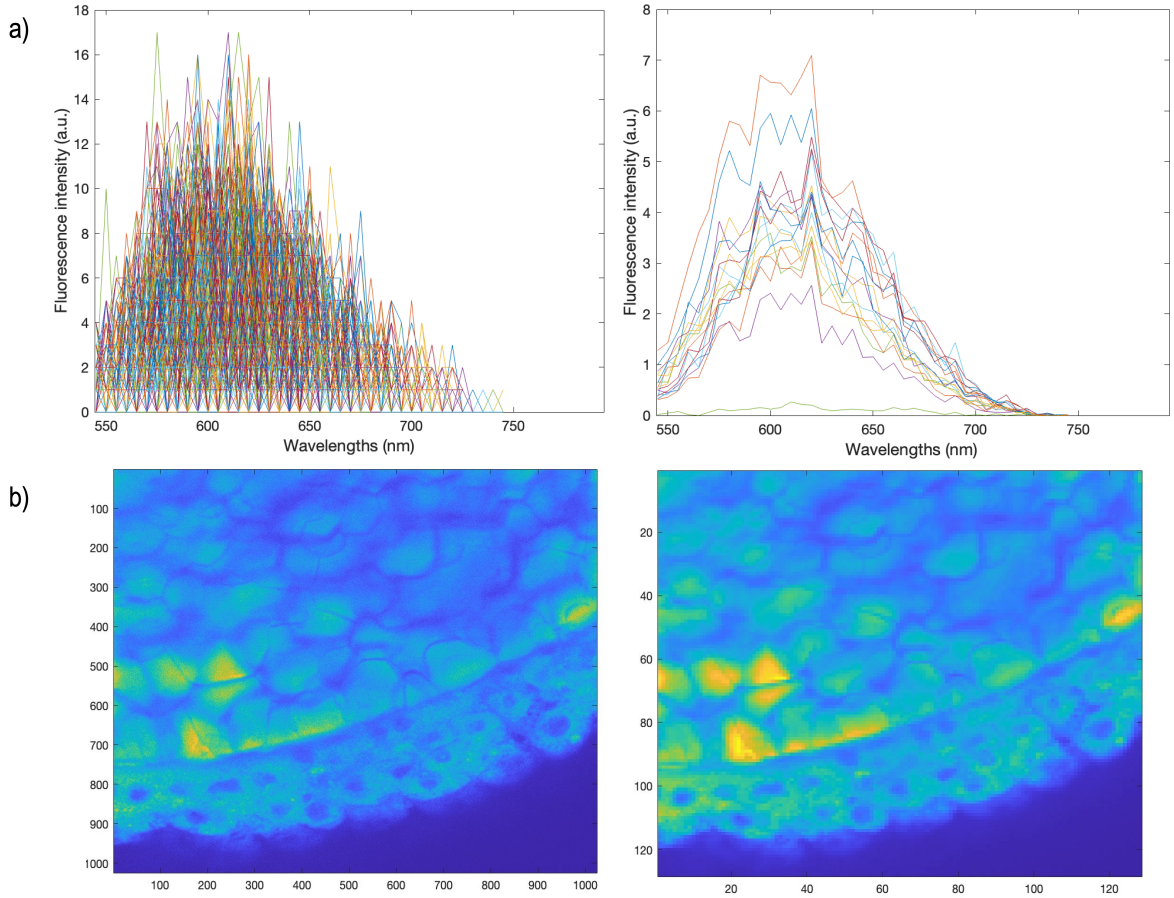

Figure 5. a) Emission spectra before (left) and after (right) the 8 x 8 binning of a Nile Red-stained embryo. b) Global intensity images before (left) and after (right) the 8 x 8 binning of a Nile Red-stained embryo.

6.2. Multivariate Curve Resolution – Alternating Least Squares (MCR-ALS)

To extract information about the stained components in the sample from the data cube, an image unmixing analysis is performed using the Multivariate Curve Resolution – Alternating Least Squares (MCR-ALS) method.[13,20]

MCR-ALS allows the characterization of each distinct fluorophore signal and the related concentration map in the scanned image. This is particularly useful when more than one fluorophore is used to label the sample or when the same fluorophore behaves in different ways depending on the biological sample environment, since the method enables the separation of the signals originating from each individual component. The method is based on a bilinear decomposition technique, inspired in the linear behaviour of the fluorescence global signal measured.

To apply MCR-ALS to a fluorescence HSI cube, the initial 3D array is unfolded into a matrix (**D**) that contains all fluorescence pixel spectra one on top of each other (as shown in Figure 6). The matrix **D** is then decomposed into the two matrices of the bilinear model in equation 1, which represent the concentration profiles (**C**) and the spectral signatures ($\mathbf{S}^T$) of the sample components. **E** is the error associated with the model. The concentration profiles are afterwards refolded intro concentration maps that recover the spatial structure of the original image.

$$D = CS^T + E \qquad \text{Equation 1}$$

After the MCR-ALS analysis, the pure emission spectra profiles and the concentration maps are obtained, allowing the identification and localisation of the distinct fluorophore components in the sample. The concentration maps are useful to distinguish in this case biological structures that have different lipidic composition and, hence, bind to different fluorophore spectral components.

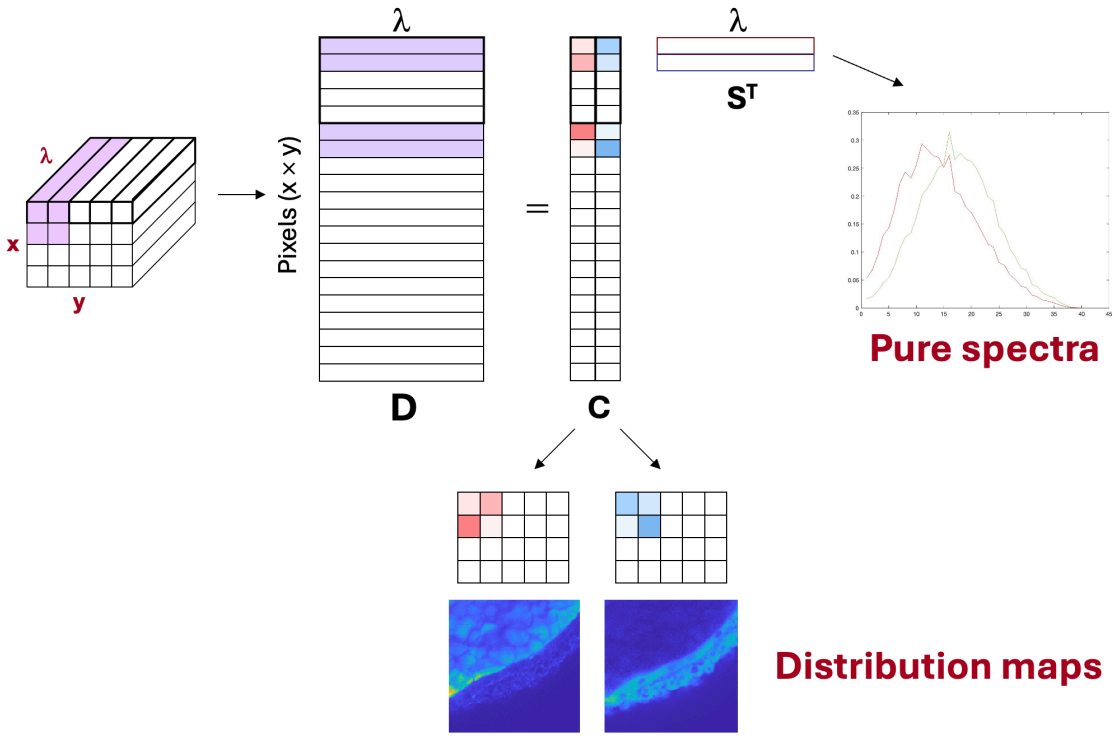

Figure 6. Representation of the MCR-ALS decomposition of a hyperspectral image data set.

Applying MCR-ALS to the fluorescence image data requires different steps. This iterative unmixing method optimizes the C and $\mathbf{S}^T$ matrices under constraints. The number of components required in the MCR model is determined using Principal Component Analysis (PCA).[21] To start the iterative optimization of **C** and $\mathbf{S}^T$, an initial estimate of the $\mathbf{S}^T$ matrix is required, with as many spectral signatures as components needed for the MCR model. This estimate is obtained from the selection of the most different emission spectra in the initial image **D** by using a Simple-to-use Interactive Self-modelling Mixture Analysis method (SIMPLISMA).[22] The method performs successive iterations to calculate the values of **C** and $\mathbf{S}^T$, considering a set of preset constraints until convergence is achieved, i.e., the model fit is not improving significantly anymore. In this study, non-negativity constraints are imposed on both concentration profiles and spectra, as both concentration values and emission fluorescence signals cannot be negative. Finally, once convergence

is reached, the final estimates of both matrices are obtained. The quality of the model was assessed through the calculation of the lack of fit (LOF (%)) and the coefficient of determination (R^2), which represents the percentage of explained variance of the MCR bilinear model. The formulas are shown in equations 2 and 3, where $d_{i,j}$ represents every element in the original data matrix **D**, and $e_{i,j}$ is the related residual associated with the MCR model (see Equation 1).

$$LOF\ (\%) = 100\sqrt{\frac{\sum_{i,j} e_{i,j}^2}{\sum_{i,j} d_{i,j}^2}} \qquad \text{Equation 2}$$

$$R^2\ (\%) = (1 - \frac{\sum_{i,j} e_{i,j}^2}{\sum_{i,j} d_{i,j}^2}) \qquad \text{Equation 3}$$

Since many samples were collected, multiset analysis was performed in order to analyse different images together and improve the results. To achieve this, the data matrices coming from the different images are arranged one on top of each other in a column-wise augmented form to build the **D** matrix, as shown in Figure 7. The related MCR model is described in equation 4. In the example presented, four images were forming the multiset.

$$[D1; D2; D3; D4] = [C1; C2; C3; C4]\ S^T + E \qquad \text{Equation 4}$$

The image blocks combined should have been acquired covering the same spectral range, although they may contain a different number of pixel rows. In this case, non-negativity constraints are also applied. Additionally, the correspondence of species constraint can be included to indicate information of presence and absence of fluorophores in the different images analysed. This last constraint is especially useful when images labelled with one or more fluorophores are present in the multiset, to indicate which of them are present in each image. Multiset analysis always leads to a better model fit and more accurate results than analysis of individual images.

As seen in Figure 7, when a column-wise augmented multiset is analysed, the final model contains a single matrix $\mathbf{S^T}$, with all the distinct spectral signatures detected in the images combined, and an augmented **C** matrix, with as many blocks as images combined. From each block in the **C** matrix, the maps of the related image can be recovered.

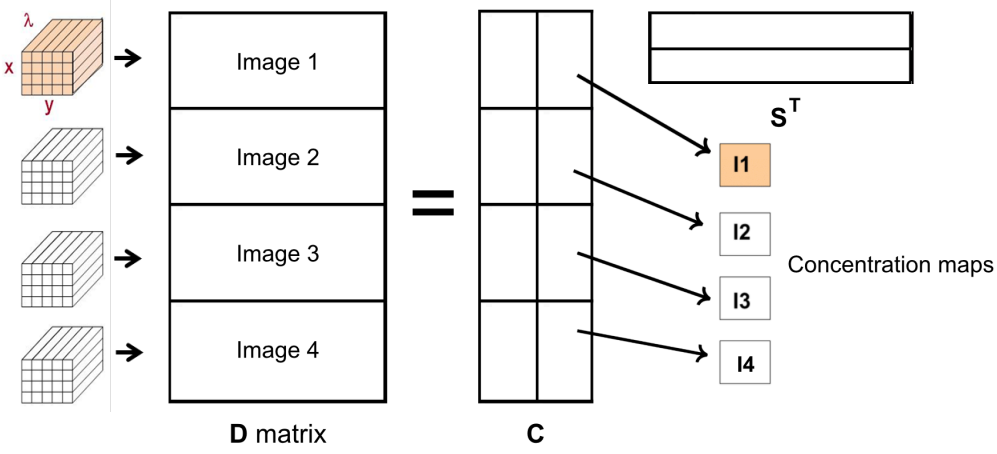

Figure 7. Representation of the data structure and MCR-ALS decomposition of an image multiset.

7. RESULTS AND DISCUSSION

7.1. EXPLORATION OF XYZ IMAGES

Single-plane xyz images were acquired to evaluate the staining quality of Nile Red and Lipi-Green fluorophores. For this purpose, the acquired images were processed using the Fiji software, adjusting contrast and brightness of the images to facilitate analysis.

For Nile Red staining, two sample groups were prepared: one group in which embryos were treated with a permeabilization and blocking solution (see section 5.1), and another group in which these steps were omitted. The aim was to evaluate whether the permeabilization and blocking solution was effective and improved the staining results as compared with no applying any of these treatments.

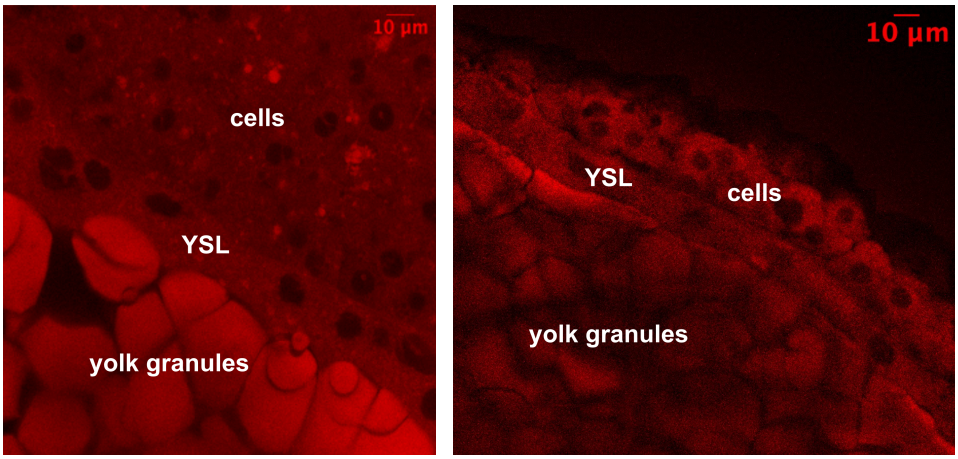

Figure 8. Acquired images of Nile Red-stained embryos. On the left, the embryo was treated with the permeabilization and blocking solution, and on the right this step was not performed.

After the image acquisition in the microscope, the visualization of two samples undergoing different treatments, as presented in Figure 8, show that both samples allowed a clear differentiation and staining of the three regions of interest, the yolk, the embryonic cells and the YSL. No significant differences in fluorophore penetration or signal quality were observed between the two groups, although a decrease in fluorescence intensity was detected in the samples that were neither permeabilized or blocked.

After staining and analysing the xyz images of embryos labelled with Nile Red and Lipi-Green and without using any treatment of any treatment of permeabilization and blocking, it was concluded that the staining quality was adequate. The results clearly showed the different parts of the embryo marked by the selected fluorophore, as illustrated in Figure 9.

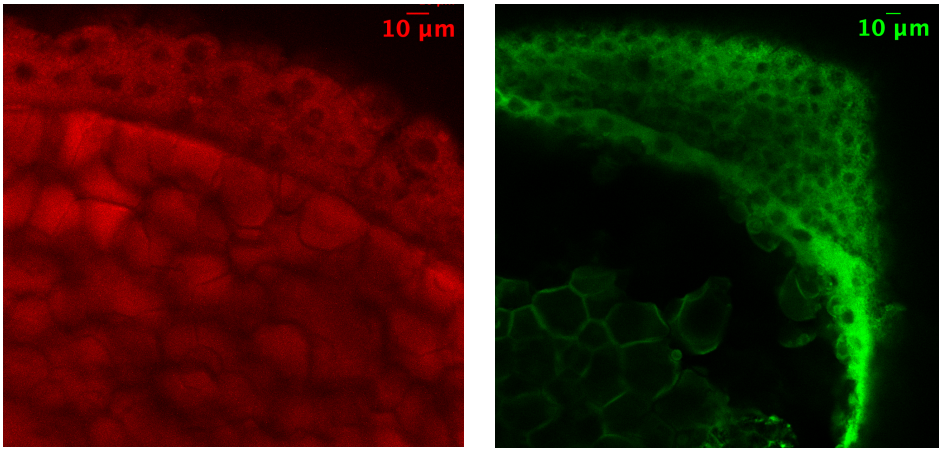

Figure 9. Acquired images of stained embryos using Nile Red (on the left) and Lipi-Green (on the right) without blocking and permeabilization.

It was concluded that the permeabilization and blocking step was not required for an effective staining, since the fluorophore was able to penetrate the embryonic structures without this treatment. Consequently, for subsequent samples, this step was omitted and embryos were directly stained with the desired fluorophore. This decision allows a milder manipulation of the embryo, which is a good option to alter as least as possible the behaviour and biological structures of the sample.

Thanks to this exploration, the first results were obtained. After analysing all the acquired images, it was observed that Nile Red effectively stained all the three different regions of the embryo. In the case of Lipi-Green, both cells and YSL appeared to be stained; however, in the yolk region, only the membrane of lipid grains was labelled, not the inside. This provided valuable information that would later be complemented by the analysis of the xyλ images. Note that with xyz images, only spatial information is noticed, but there is no possibility to investigate whether a single fluorophore can stain in a different manner lipids of different composition.

7.2. ANALYSIS OF XYΛ IMAGES

This section presents the results obtained from different stained embryos using Nile Red, Lipi-Green and a combination of both fluorophores. Remember that xyλ images associate a full emission spectrum with every pixel. In this context, embryos were first dyed with each fluorophore individually, to understand better their staining patterns and lipid affinity. Following that, they were stained with both fluorophores simultaneously. The combined fluorescence signals were then separated using MCR-ALS analysis, allowing the contribution of each fluorophore to be evaluated independently. Table 1 summarises a set of selected images acquired with their codes and their main characteristics.

Table 1. Images acquired in xyλ mode using the different fluorophores and spectral channels.

Image code	**Image**(*)	**Dye(s) used**	**λ excitation** [nm]	**λ emission** [nm]
NR1	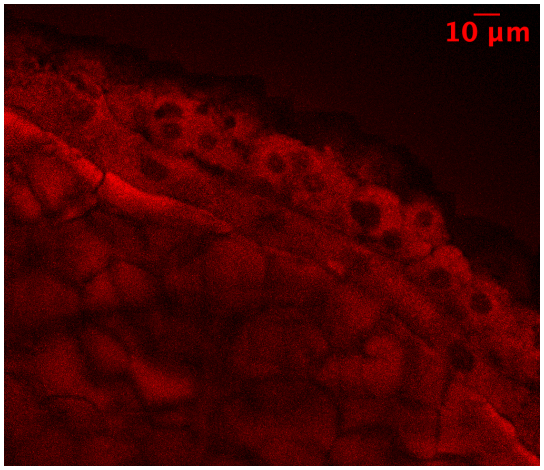	Nile Red	532	545-745
NR2	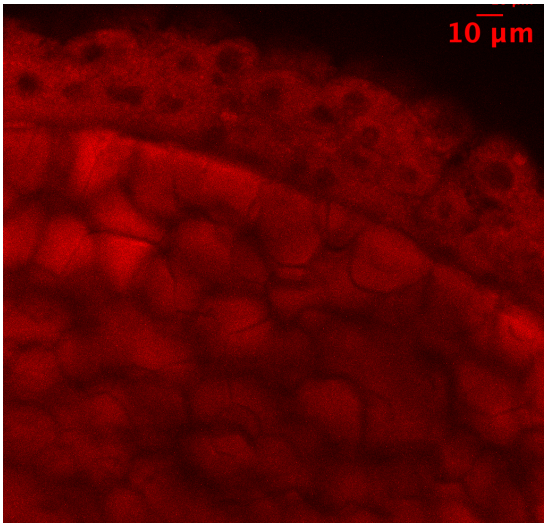	Nile Red	532	545-745

Image code	Image(*)	Dye(s) used	λ excitation [nm]	λ emission [nm]
NR3	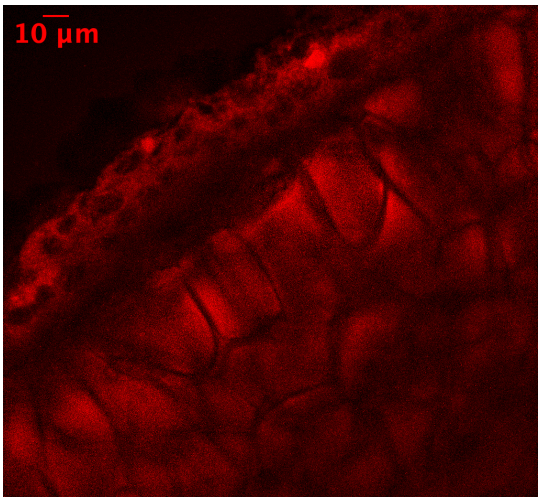	Nile Red	532	545-745
LG1	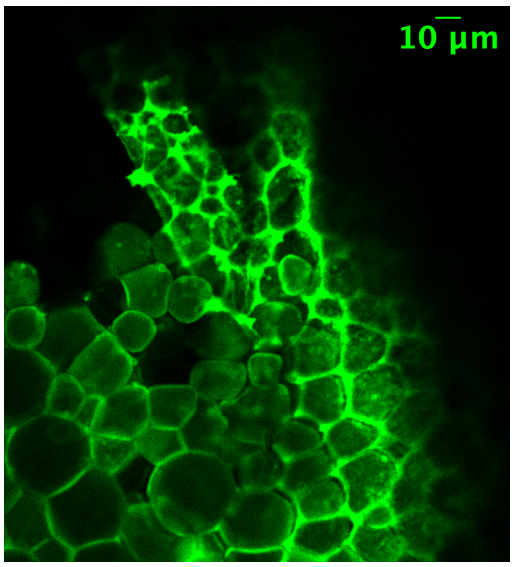	Lipi-Green	498	510-745
LG2	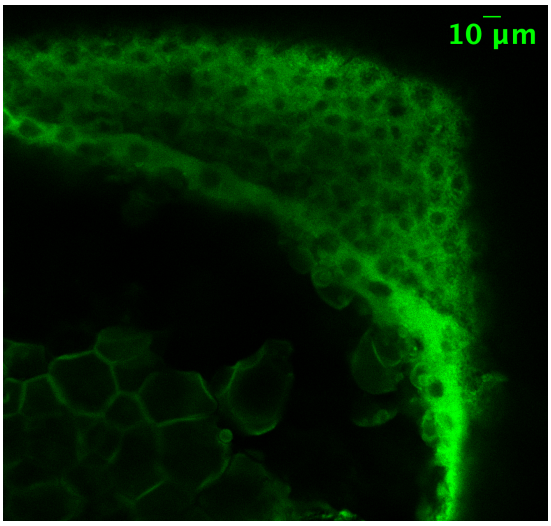	Lipi-Green	498	510-745

Image code	Image(*)	Dye(s) used	λ excitation [nm]	λ emission [nm]
NRLG1	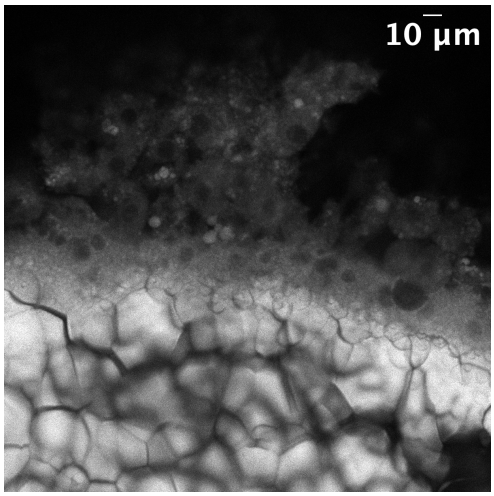	Nile Red and Lipi-Green	498	510-745
NRLG2	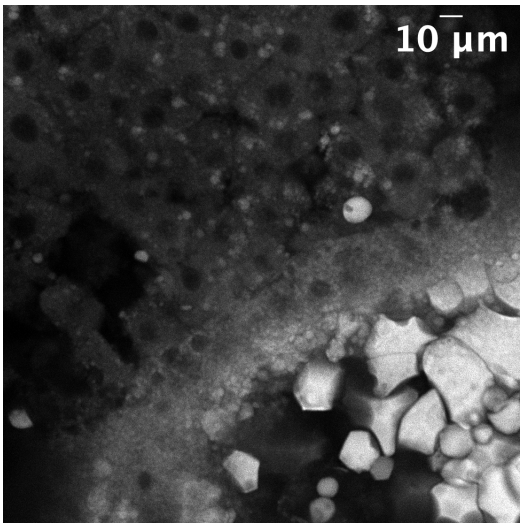	Nile Red and Lipi-Green	498	510-745
NRLG3	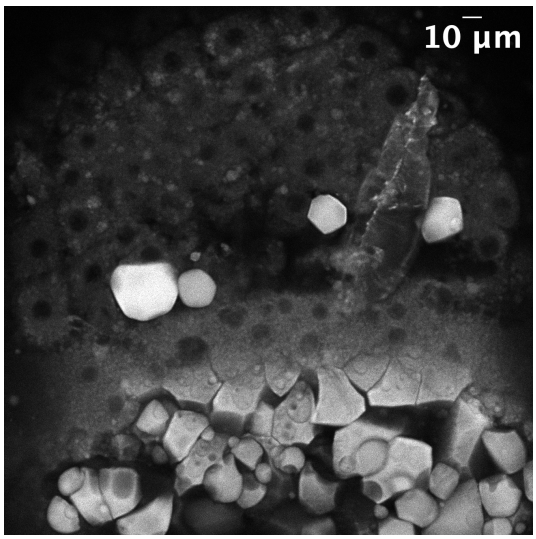	Nile Red and Lipi-Green	498	510-745

(*) Note that all images presented are obtained through the integration of all fluorescence intensities obtained at the different wavelengths in the emission spectrum of every pixel.

Below, the results of the application of the image unmixing analysis carried out by MCR-ALS to an individual image and to diverse multisets formed by several labelled samples are presented. Table 2 summarises the structure of the data sets analysed, and the main parameters of the MCR-ALS models obtained. In all analyses, the parameters related to variance explained and lack of fit were satisfactory and in accordance with the noise level of the emission spectra of the images. In all analyses, the non-negativity constraint was used in both the matrix of concentration profiles and the matrix of pure spectra (see section 6.2).

Table 2. Data structures and main MCR-ALS results of the analysis of the images studied.

Data set	**Nr of components**	**LOF** (%)	**R^2** (%)
NR1	2	7.4677	99.4423
[NR1;NR2;NR3]	2	6.601	99.5643
[LG1;LG2]	1	12.05	98.548
[NR1;LG1;NRLG1]	3	13.793	98.0975
[NR1;LG1;NRLG2]	3	14.3775	97.9329
[NR1;LG1;NRLG3]	3	14.9627	97.7612

7.2.1. Analysis of Nile Red stained embryos

Nile Red belongs to a class of fluorescent molecules that exhibit changes in their emission spectra in response to the polarity of the local environment, a property referred to as solvatochromism. In previous studies, it has been reported that different emission spectral signatures could be potentially distinguished depending on the chemical polarity of the lipid environment, making it useful for distinguishing between lipidic components using a single dye.[11]

MCR-ALS analysis was performed on the single image NR1, and two distinct components were obtained, showing that there were zones in the zebrafish embryo with lipids of different nature. Figure 10 shows the pure distribution maps of these two components, one related to the cells and YSL (on the right), while the other was associated with the yolk (on the left).

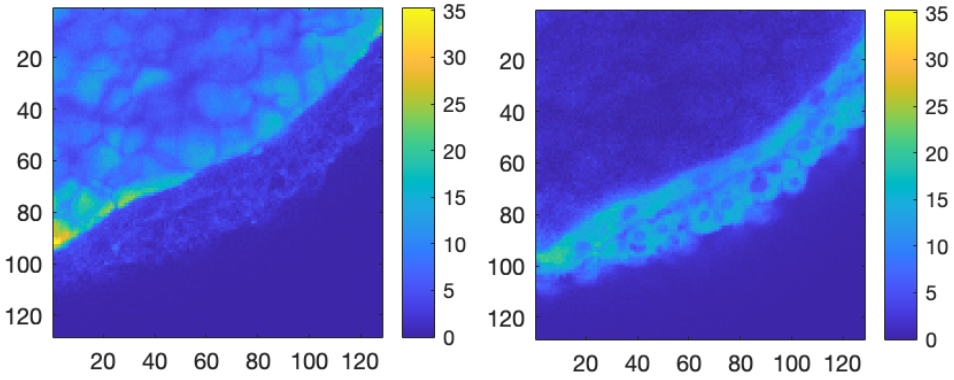

Figure 10. Pure distribution maps of Nile Red-stained embryos from image NR1 obtained by MCR-ALS analysis.

Figure 11 presents the MCR-ALS results as they will be shown throughout this section. On the left, the pure distribution maps obtained in the previous Figure 10 are overlaid for a better visualization to help in the location and overlap among components. On the right, the related pure spectral signatures, using the same colour code for the analogous components, are presented. In this way, both the spatial information (coming from the **C** matrix, as described in section 6.2), and chemical information (from the $\mathbf{S}^T$ matrix) are summarized in a single figure. As observed before, the two regions clearly distinguished in the maps of the previous Figure 10 show no overlap between them in any part. The lipid component displayed in green, related to the YSL and the cells, correspond to more polar lipids species, since these structures are mainly constituted by phospholipids. In the related spectral signature, the maximum peak in the emission shift of them is around 635 nm, as seen in Figure 11. However, the lipids in the red region, related to the yolk, correspond to less polar lipids, basically triacyclglycerols, which are neutral lipids. The emission maximum of this component is around 585 nm. This demonstrates that staining more polar lipids results in a less intense emission at longer wavelengths.

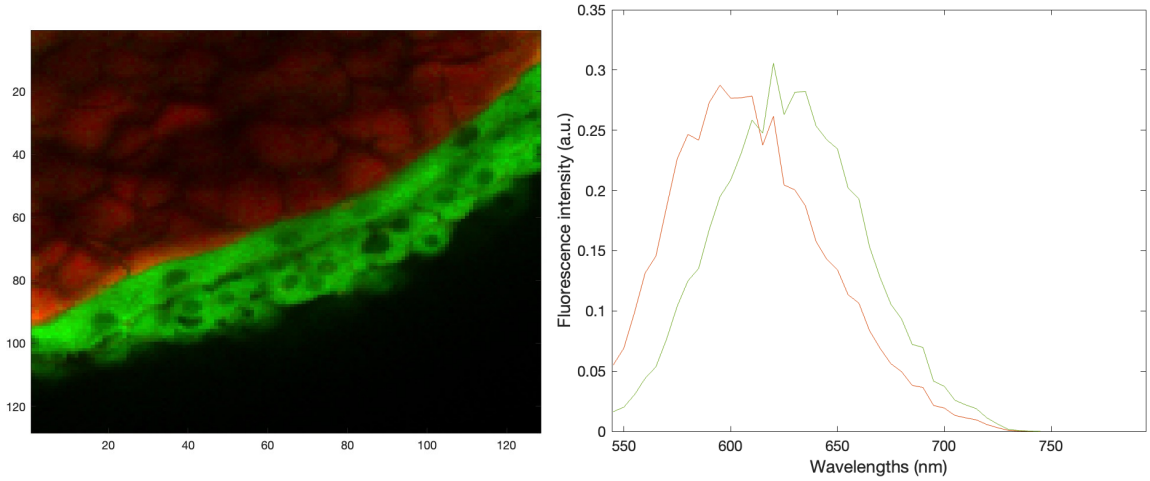

Figure 11. Left plot: overlaid maps of the two different components in Nile Red-stained embryos from image NR1. Right plot: pure emission spectra of both components. The red spectrum corresponds to the yolk and the green spectrum, to the YSL and cells.

The consistency of these results was tested performing an MCR-ALS multiset analysis including all images stained with this dye. Hence, the **D** matrix was constructed using images NR1, NR2 and NR3, arranged one on top of the other, as explained in section 6.2. The result of a multiset analysis formed by a column-wise augmented matrix is a single $\mathbf{S}^T$ matrix, with the pure spectra valid for all images analysed, and as many blocks in the **C** matrix as images analysed. In the presented analysis, it means that the **C** matrix will be formed by three blocks and, therefore, three sets of maps can be derived, one per each image analysed, as shown in Figure 12.

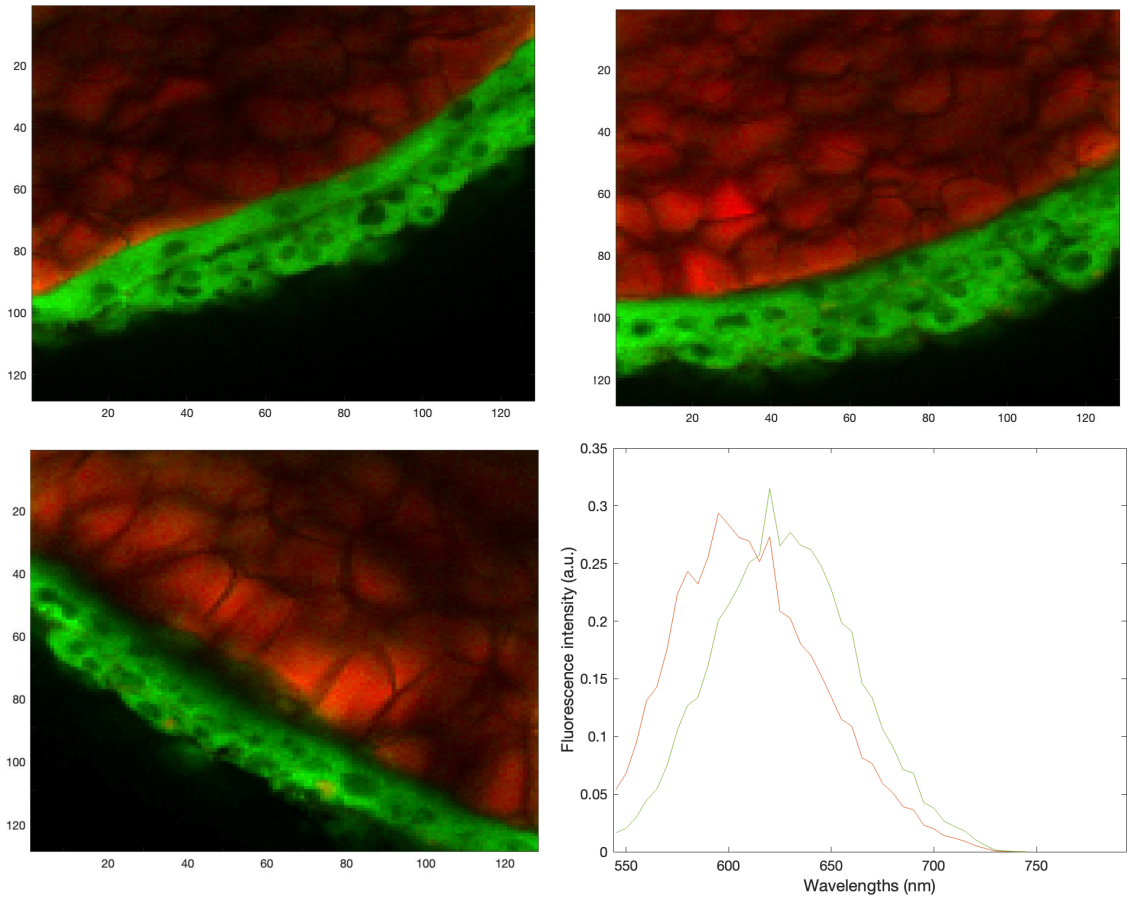

Figure 12. Overlapped maps of the two different components in Nile Red-stained embryos from images NR1, NR2 and NR3, and the pure emission spectra of both components. The red spectrum corresponds to the yolk and the green spectrum, to the YSL and cells.

The results obtained confirm the need of two components to describe the behaviour of the images analysed. The overlaid maps of the two components in the three images show the consistency of the results, since the same zones (yolk in red and YSL and animal

cells in green) are clearly separated in all of them. It is important to note that the images come from different embryos, thus indicating that the results show a tendency present in the different samples analysed and are not linked to a single individual behaviour. The pure spectral signatures are also in agreement with those obtained in the analysis of the individual image NR1. Furthermore, no distinct behaviour is observed between the YSL and the embryonic cells, suggesting that this fluorophore is unable to differentiate between these two regions. This is likely due to their similar polarity, in contrast to the yolk, which presents a different lipid environment, and is clearly distinguished.

7.2.2. Analysis of Lipi-Green stained embryos

The other fluorophore used in this study was Lipi-Green. In other studies, it was known that this dye stains lipid droplets, which are formed by neutral lipids such as triacylglycerol and cholesterol esters surrounded by a phospholipid monolayer.[10] Based on this property, it was expected that Lipi-Green would preferentially stain the interior of yolk granules, since they contain a higher proportion of neutral lipids than the cells.

The MCR-ALS multiset analysis was performed in this case on images LG1 and LG2. However, in contrast to the results obtained with Nile Red, only one component was identified. This component was localised mainly at the membrane of yolk granules, rather than in their interior, and it was also detected in the YSL and the cells, as shown in Figure 13. The emission spectrum is shown in Figure 14.

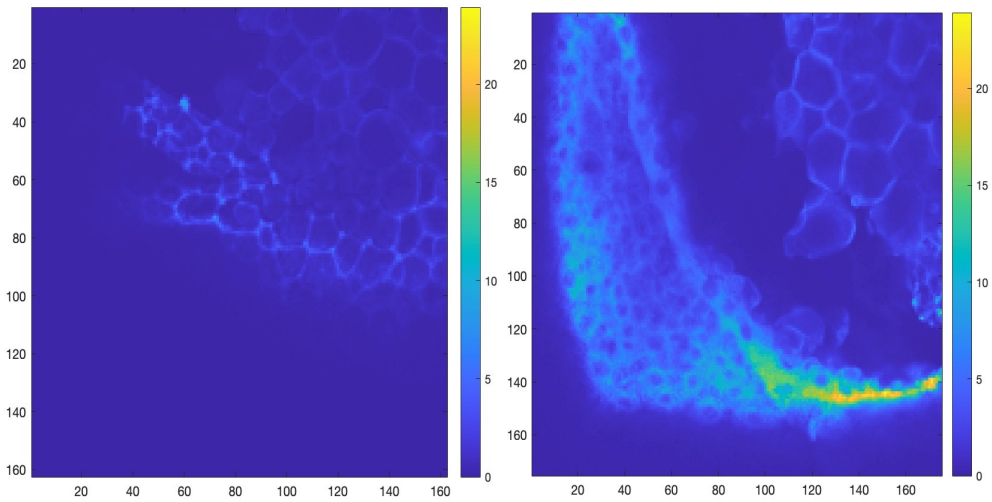

Figure 13. Pure distribution maps of Lipi-Green-stained embryos from images LG1 and LG2.

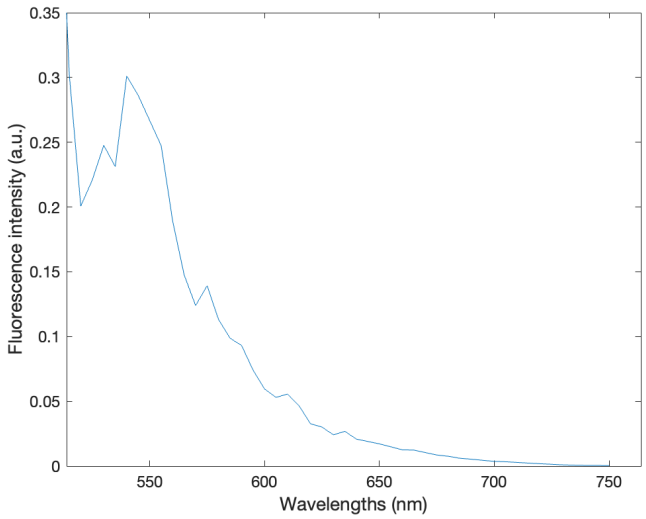

Figure 14. Emission spectrum of Lipi-Green obtained by MCR-ALS multiset analysis from images LG1 and LG2.

The results did not fully match the expected results. In the case of the cells, it was concluded that higher spatial resolution would be required to determine whether the dye is specifically labelling lipid droplets inside the cells, as this could not be clearly determined

under the current conditions. Regarding the membrane staining, both in the animal cells and the yolk granules, some articles reported that this dye preferentially labels the surface of spherical intracellular structures, which is consistent with the observations made in this study. Specifically, in the zebrafish yolk, studies using a membrane-GFP transgenic line, have shown a clear membrane surrounding the yolk granules, as in the cell membranes.[23] The fluorescence behaviour reported in that article matches qualitatively well with the type of staining of Lipi-Green observed in this work. Little is known about yolk granules composition, but altogether suggests that Lipi-Green preferentially associates with lipid-rich membranes. From a biophysical perspective, previous work has described the yolk content as a viscous Newtonian fluid, while the yolk surface behaves as an extremely soft solid. This dual mechanical behaviour may be related to the structural organization of the yolk granules and their surrounding membranes, providing a possible explanation for the preferential membrane-associated staining observed with Lipi-Green.

7.2.3. General image analysis of single and multistained zebrafish embryos

To obtain more accurate results and understand better the lipidic composition of the samples, embryos were also stained simultaneously with both fluorophores. MCR-ALS multiset analysis was then performed by constructing the **D** matrix using one image stained only with Nile Red, another stained only with Lipi-Green, and a third image where both fluorophores were present in the same sample, as shown in Figure 15. To enable the construction of this multiset, all images were combined considering only the spectral range 545-745 nm, common to all images analysed.

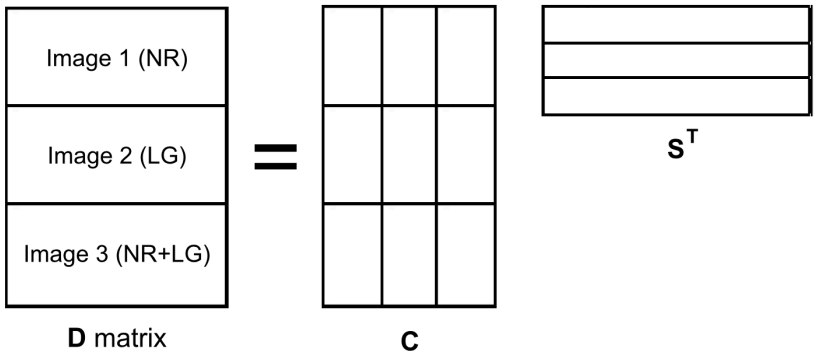

Figure 15. Representation of the MCR-ALS decomposition of the multiset.

In this case, it is particularly relevant to use the correspondence of species constraint, which provides information about the presence or absence of compounds in the different images. This constraint helps improving the results and increasing the accuracy of the analysis. The way to encode this information is using in this case a 3 x 3 matrix, in which the columns represent the three different components found in the analysis, and the rows correspond to each of the images in the multiset. If the component is present in a given image, a value of 1 is assigned, otherwise a value of 0 is used. The correspondence of species matrix applied in the multiset analysis is shown in Figure 16. When this constraint is applied, the concentration profiles related to absent contributions in images are set to zero. The fact of introducing less mixed information in the multiset, i.e., the images where only one dye is present, facilitate the definition of the related pure spectral signatures associated with these components and, hence, help to clarify the behaviour of the most complex image in the multiset structure, i.e., the one with both dyes.

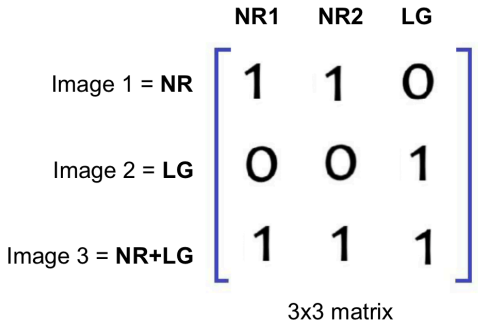

Figure 16. Correspondence of species matrix related to multiset in Figure 15.

In this multiset analysis, three components were required, as expected in the previous analyses in sections 7.2.1 and 7.2.2. In all the multisets analysed, the model fit parameters were satisfactory. The pure spectral signatures obtained in the three independent multisets, where a different sample labelled with two fluorophores was used every time, were in a very close agreement with one another. Therefore, for the sake of simplicity, only one set of pure spectral signatures will be presented. Likewise, the pure distribution maps of the images stained with a single dye in the multiset agree with those presented in the previous sections. Therefore, only the maps related to samples stained with both Nile Red and Lipi-Green will be shown in this section.

The spectra of the three different components are shown in Figure 17. When compared with the single-stained samples, the emission spectra exhibit the same shape. The red spectrum corresponds to the Lipi-Green dye, emitting at lower wavelengths, while the green and blue spectra are associated with the Nile Red dye, which displays two distinct emission shifts, as previously explained. In order to facilitate visualization, each spectrum is shown using the same colour assigned to the corresponding component in the distribution map.

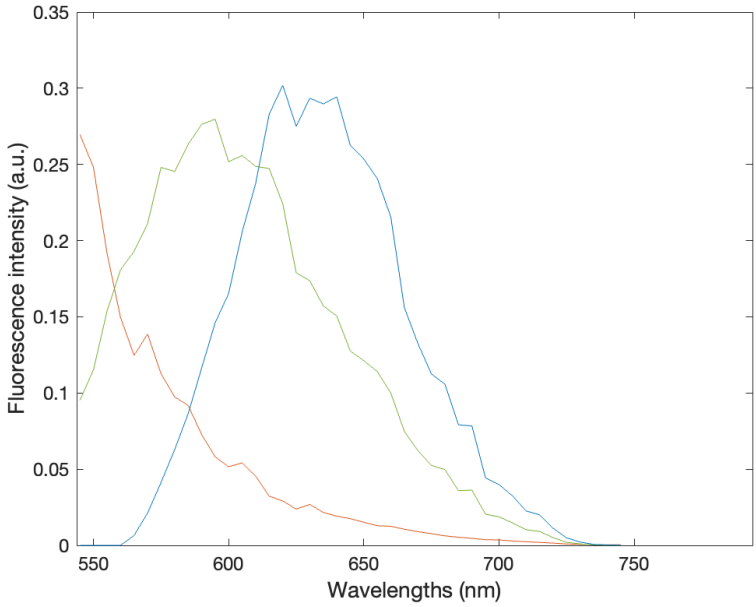

Figure 17. Emission spectra of Lipi-Green and Nile Red obtained by MCR-ALS multiset analysis.

As in the single-stained embryos, the results were obtained as pure distribution maps, which were later overlaid into a single map to facilitate visualization and comparison, shown in Figure 18 and 19.

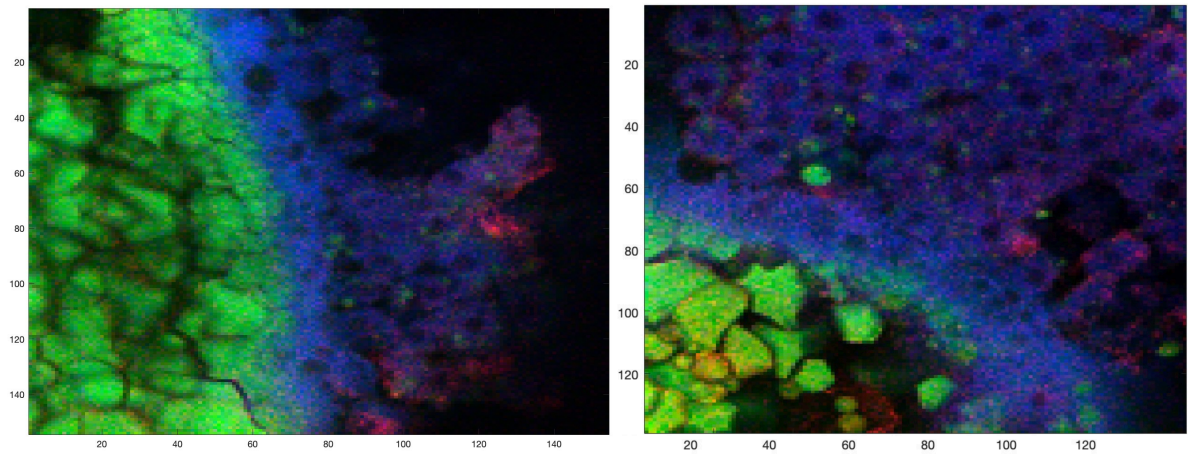

Figure 18. Overlapped maps obtained from MCR-ALS multiset performed using images NR1, LG1 and NRLG1 (left) and NRLG2 (right).

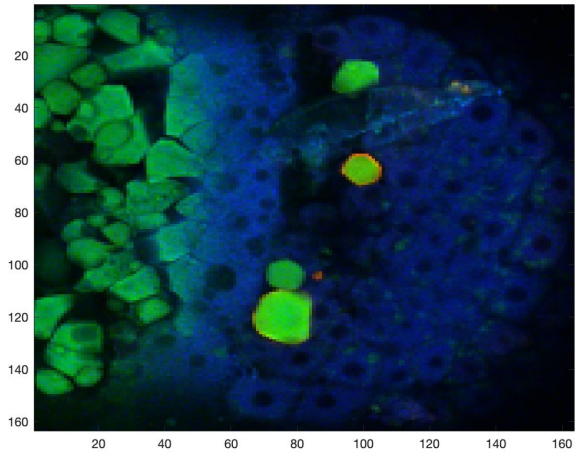

Figure 19. Overlapped map obtained from MCR-ALS multiset performed using images NR1, LG1 and NRLG3.

The three different components are clearly identified: the blue region corresponds to the cells and YSL stained by Nile Red, the green region corresponds to the yolk granules stained by Nile Red, and the red regions correspond to the components stained by Lipi-Green, mainly observed in the cellular regions and between yolk granules. Nile Red is observed to stain the interior of the yolk granules, whereas Lipi-Green predominantly labels their membranes. As observed, the results are consistent with the expectations, as they follow the same staining patterns as the single-stained multiset analysis shown before.

In the case of Lipi-Green, the results obtained from the multiset analysis appear more meaningful than those from the single-stained ones. In this case, not all the cells are uniformly stained, instead, only single spots are observed, which may correspond to lipid droplets found in cells. To confirm this hypothesis, apart from improving the spatial resolution, the staining procedure should be performed again, changing the staining sequence of the fluorophores, as interactions between fluorophores may influence the results. The reduced cellular staining by Lipi-Green observed in the multiset analysis could reflect a more accurate localization, or alternatively, competition between the two fluorophores, leading to the displacement of the first one applied, Lipi-Green.

8. CONCLUSIONS

The main objective of this study was to understand the lipidic distribution during zebrafish embryonic development, specifically at middle-epiboly stage. To achieve this goal, hyperspectral imaging combined with chemometric analysis using MCR-ALS was applied to embryos stained with different lipid-selective fluorophores.

Firstly, the adequacy of Nile Red and Lipi-Green as lipid markers in zebrafish embryos was evaluated. After the staining procedure and subsequent analysis of the acquired hyperspectral images, it was observed that Nile Red successfully stained the three regions of the embryo (YSL, cells and yolk). However, Lipi-Green only stained the cells and YSL, as well as the membrane of the yolk granules, but not their interior.

Using MCR-ALS, the distinct components present in the embryos were able to be separated. For Nile Red, two different components were identified: one associated with the yolk and another corresponding to the cells and the YSL, exhibiting two emission spectral signatures depending on the polarity of the lipidic environment. This is a significant advantage, since it allows the differentiation of two distinct regions by just using one fluorophore. Thus, the yolk was associated with less polar lipids, whereas the cells and YSL to lipids of higher polarity. This different environment caused an emission shift to higher wavelengths as lipid polarity increases. In contrast, Lipi-Green only labelled a single component, which appeared in specific parts across all three embryonic regions, mainly on yolk or cell membranes and interstitial spaces.

By combining HSI and MCR-ALS analysis, the three main parts of the embryo and three components were successfully distinguished. This chemometric approach proved to be a powerful tool for extracting meaningful information from complex hyperspectral images, allowing the identification of pure spectral signatures and their corresponding spatial distributions. Furthermore, it was noticed that the use of multiset analysis instead of single-images analysis improved the LOF and R^2 values, enhancing the accuracy of the results.

Finally, this study could be extended by testing different fluorophores capable of distinguishing between the cells and YSL, which are very similar in composition, or by increasing the spatial resolution to better characterize the fluorophore labelling. These improvements would contribute to a deeper understanding of the lipidic distribution and embryonic development in zebrafish.

9. REFERENCES AND NOTES

1. Choi, TY.; Choi, TI.; Lee, YR.; Choe, SK.; Kim, CH. *Zebrafish as an animal model for biomedical research*. Exp. Mol. Med. **2021**, 53, 310-317. https://doi.org/10.1038/s12276-021-00571-5
2. *The Barcelona Medical Photonics Network: united to improve the health and well-being of society*. ICFO News, February 18, **2021** https://www.icfo.eu/news/1858/the-barcelona-medical-photonics-network-united-to-improve-the-health-and-well-being-of-society (accessed Nov 13, 2025).
3. Burke, E. *Why Use Zebrafish to Study Human Diseases?* NIH Intramural Research Program Blog, August 9, **2016** https://irp.nih.gov/blog/post/2016/08/why-use-zebrafish-to-study-human-diseases (accessed Nov 18, 2025).
4. Kimmel, C.B.; Ballard, W.W.; Kimmel, S.R.; Ullmann, B.; Schilling, T.F. *Stages of Embryonic Development of the Zebrafish*. Dev. Dyn. **1995**, 203 (3), 253-310. https://doi.org/10.1002/aja.1002030302
5. Carvalho, L.; Heisenberg, C.P. *The Yolk Syncytial Layer in Early Zebrafish Development.* Trends Cell Biol. **2010**, 20 (10), 586-592. https://doi.org/10.1016/j.tcb.2010.06.009
6. Bruce, A. E. E. *Zebrafish Epiboly: Spreading Thin over the Yolk.* Dev. Dyn. **2016**, 245 (3), 244-258. https://doi.org/10.1002/dvdy.24353
7. *Epiboly*. Wikipedia: The Free Encyclopedia. https://en.wikipedia.org/wiki/Epiboly (accessed Dec 8, 2025)
8. Ho, S.Y.; Thorpe, J.L.; Deng, Y.; Santana, E.; DeRose, R.A.; Farber, S.A. *Lipid Metabolism in Zebrafish.* Methods Cell Biol. **2004**, 76, 87-108. https://doi.org/10.1016/S0091-679X(04)76006-9
9. Shihana, F.; Manuneedhi Cholan, P.; Fraser, S.; Oehlers, S.H.; Seth, D. *Investigating the Role of Lipid Genes in Liver Disease Using Fatty Liver Models of Alcohol and High Fat in Zebrafish (Danio rerio)*. Liver Int. **2023**, 43 (11), 2455-2468. https://doi.org/10.1111/liv.15716
10. Lee, J.H.; So, J.H.; Jeon, J.H.; Choi, E.B.; Lee, Y.R.; Chang, Y.T.; Kim, C.H.; Bae, M. A.; Ahn, J. H. *Synthesis of a New Fluorescent Small Molecule Probe and Its Use for In Vivo Lipid Imaging*. Chem. Commun. **2011**, 47, 4527-4529. https://doi.org/10.1039/c1cc11253h
11. Teo, W.; Caprariello, A.V.; Morgan, M.L.; et al. *Nile Red Fluorescence Spectroscopy Reports Early Physicochemical Changes in Myelin with High Sensitivity*. Proc. Natl. Acad. Sci. U.S.A. **2021**, 118 (8), e2016897118. https://doi.org/10.1073/pnas.2016897118
12. *LD02 Product Information*. Dojindo Molecular Technologies, Inc. https://www.dojindo.com/EUROPE/products/LD02/ (accessed Jan 3, 2026).
13. de Juan, A.; Tauler, R. *Multivariate Curve Resolution: 50 Years Addressing the Mixture Analysis Problem – A Review*. Anal. Chim. Acta. **2021**, 1145, 59-78. https://doi.org/10.1016/j.aca.2020.10.051
14. Marsal, M.; Hernández-Vega, A.; Pouille, P.A.; Martin-Blanco, E. *Rab5ab-Mediated Yolk Cell Membrane Endocytosis Is Essential for Zebrafish Epiboly and Mechanical Equilibrium During Gastrulation*. Front. Cell Dev. Biol. **2021**, 9, 697097. https://doi.org/10.3389/fcell.2021.697097
15. *Leica TCS SP8 STED 3X-FALCON*. ICFO Research Facilities. https://www.icfo.eu/research/facilities/sln/leica-tcs-sp8-sted-3x-falcon/ (accessed Oct 20, 2025).
16. *Fluorescence SpectraViewer*. Thermo Fischer Scientific. https://www.thermofisher.com/order/fluorescence-spectraviewer/?SID=srch-svtool&UID=1142lip#!/ (accessed Dec 18, 2025).
17. *LD01/LD02/LD03/LD04 Product Manuals*. Dojindo Molecular Technologies, Inc. https://www.dojindo.com/manual/LD01_LD02_LD03_LD04/ (accessed Jan 3, 2026).
18. Amigo, J.M.; Babamoradi, H.; Elcoroaristizabal, S. *Hyperspectral Image Analysis: A Tutorial*. Anal. Chim. Acta. **2015**, 896, 34-51. https://doi.org/10.1016/j.aca.2015.09.030
19. Kurz, W.; Wang, K.; Bektas, F.; et al. *Dimensionality Reduction in Hyperspectral Imaging Using Standard Deviation-Based Band Selection for Efficient Classification*. Sci. Rep. **2025**, 15, 34478. https://doi.org/10.1038/s41598-025-21738-4
20. Jaumot, J.; de Juan, A.; Tauler, R. *MCR-ALS GUI 2.0: New Features and Applications*. Chemometrics and Intelligent Laboratory Systems. **2015**, 140, 1-12. https://doi.org/10.1016/j.chemolab.2014.10.003
21. Jolliffe, I.T. *Principal Component Analysis, 2nd ed.*; Springer Series in Statistics; Springer: New York, NY, **2002**. https://doi.org/10.1007/b98835
22. Windig, W.; Guilment, J. *Interactive Self-Modeling Mixture Analysis*. Anal. Chem. **1991**, 63 (14), 1425-1432. https://doi.org/10.1021/ac00014a016
23. Hernández-Vega, A.; Marsal, M.; Pouille, P.A.; Tosi, S.; Colombelli, J.; Luque, T.; Navajas, D.; Pagonabarraga, I.; Martín-Blanco, E. *Polarized Cortical Tension Drives Zebrafish Epiboly Movements*. EMBO J. **2017**, 36 (1), 25-41. https://doi.org/10.15252/embj.201694264

APPENDICES

APPENDIX 1: FLUOROPHORES SPECTRA

Nile Red: excitation (dotted line) and emission (continuous line) spectra of triglyceride (yellow) and phospholipids (red).

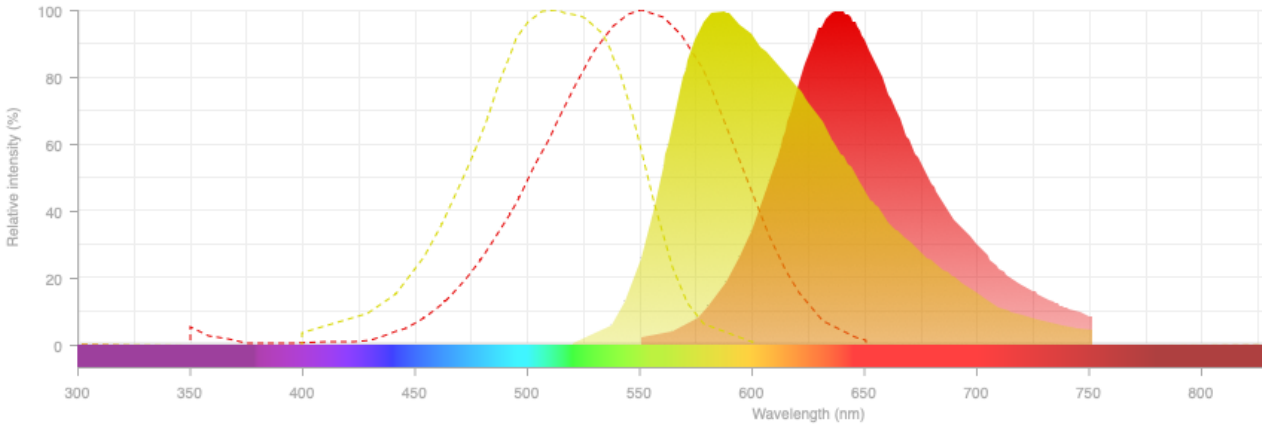

Lipi-Green: excitation (dotted line) and emission (continuous line) spectra of the dye.